Interaction of an edge dislocation with voids in α-iron modelled with different interatomic potentials

2008 J. Phys.: Condens. Matter 20 445007

(http://iopscience.iop.org/0953-8984/20/44/445007)

IOP Publishing Journal of Physics: Condensed Matter

J. Phys.: Condens. Matter **20** (2008) 445007 (11pp) doi:10.1088/0953-8984/20/44/445007

Interaction of an edge dislocation with voids in α-iron modelled with different interatomic potentials

D Terentyev[1,4], D J Bacon[2] and Yu N Osetsky[3]

[1] SCK-CEN, Nuclear Material Science Institute, Boeretang 200, B-2400, Mol, Belgium
[2] Department of Engineering, The University of Liverpool, Brownlow Hill, Liverpool L69 3GH, UK
[3] Material Science and Technology, ORNL, Oak Ridge, TN 37831, USA

E-mail: dterenty@sckcen.be

Received 8 April 2008, in final form 18 September 2008
Published 10 October 2008
Online at stacks.iop.org/JPhysCM/20/445007

Abstract

Atomic processes and strengthening effects due to interaction between edge dislocations and voids in α-iron have been investigated by means of molecular dynamics with a recently developed interatomic potential (Ackland *et al* 2004 *J. Phys.: Condens. Matter* **16** S2629) and compared with those obtained earlier with an older potential (Ackland *et al* 1997 *Phil. Mag.* A **75** 713). Differences between the interactions for the two models are insignificant at temperature $T \geqslant 100$ K, thereby confirming the validity of the previous results. In particular, voids are relatively strong obstacles because for large voids and/or low temperature, the initially straight edge dislocation is pulled into screw orientation before it breaks away at the critical shear stress, τ_c. Differences between the core structures and glide planes of the $1/2\langle 111\rangle$ screw dislocation for the two potentials do not affect τ_c in this temperature range. The only significant difference between the dislocation–void interactions in the two models occurs at low temperature in static or pseudo-static conditions ($T \leqslant 1$ K). It arises from the influence of the dislocation segment in the 70°-mixed orientation with the (Ackland *et al* 2004 *J. Phys.: Condens. Matter* **16** S2629) potential and is seen in the critical line shape at which the dislocation breaks from the void. It affects τ_c for some combinations of void size and spacing. The effect on the line shape does not arise from anisotropy of the elastic line tension: it is due to the high Peierls stress of the 70° dislocation. When this effect does not control breakaway, the dependence of τ_c on void size and spacing follows an equation first found by modelling the Orowan process in the approximation of linear elasticity.

(Some figures in this article are in colour only in the electronic version)

1. Introduction

An understanding of radiation-induced phenomena in the structural materials such as reactor pressure vessel steels is necessary for predictive modelling of property changes and performance of nuclear power plant. The damage that produces changes brought about by radiation is created at the nano-scale. Thus, in the context of the development of a multi-scale modelling approach, which treats and links phenomena across a wide range of spatial and temporal scales, atomic-level simulation is particularly important because it can provide not only detailed understanding of mechanisms that control properties but also quantitative information for higher-level analysis and simulation based on the continuum approximation. With regard to mechanical properties such as the yield stress, the dominant process of concern is the effect of radiation damage on dislocations gliding under stress. Atomic-level computer simulation by molecular dynamics (MD) has been reported already for obstacles to glide in iron such as voids, interstitial loops and copper precipitates, e.g. [1–11]. This work has exposed a plethora of mechanisms,

[4] Author to whom any correspondence should be addressed.

such as obstacle shearing, absorption and transformation, and demonstrated that their dependence on temperature, applied stain rate and obstacle size could only be determined by simulation.

Yielding in unirradiated iron crystals below 300 K is governed by the mobility of screw dislocations, e.g. [12], but above that range edge dislocations are also important, particularly when obstacles to slip are present. In addition to their role in yielding, they have a significant role in absorbing defects from the matrix. In fact, previous atomic-level modelling has concentrated on the interaction of edge dislocations with damage. This is partly because the edge dislocation requires simpler boundary conditions in an MD model and is more readily simulated, and also because the validity of many of the interatomic potentials available for iron is questionable as far as screw dislocation core structure and behaviour are concerned.

This paper focuses on the obstacle strength of voids in iron and the atomic mechanisms that control breakaway of a dislocation from a void. Recent dislocation dynamics modelling based on the continuum approximation has indicated that voids provide the main contribution to strengthening in irradiated ferritic low-carbon steel [13]. As in previous work on this problem [2–6], we treat the edge dislocation. The background behind revisiting this topic is explained in the following section.

2. Background: void strengthening in iron

Previous atomic-level simulation studies showed four main features of voids as obstacles to a $1/2\langle 111\rangle\{110\}$ edge dislocation gliding under a resolved shear stress, τ, in BCC iron.

(a) Voids larger in diameter than $\sim$2 nm are 'strong' obstacles, for when the dislocation bows out between voids under increasing τ, the segments on either side of the voids move into parallel alignment, i.e. they adopt a dipole configuration, which is the critical shape in the Orowan mechanism. The critical (maximum) stress, τ_c, is reached when the drawn-out screw dipole breaks free of a void.

(b) The dependence of τ_c on void diameter, D, and centre-to-centre spacing, $L+D$, for a periodic row of voids in a crystal at 0 K fits the relation

$$\tau_c = \frac{Gb}{2\pi L}\left[\ln\left(D^{-1}+L^{-1}\right)^{-1}+B\right] \qquad (1)$$

at temperature $T = 0$ K. This equation was found in [14, 15] from simulation with a model of a flexible dislocation passing through a row of voids in a continuum. Here, G is the shear modulus consistent with the energy pre-factor for a straight screw dislocation and b is the magnitude of the Burgers vector. B is a constant that depends on the nature of the strong obstacle: it was found to range from 0.7 for impenetrable obstacles to 1.52 for voids. L and D are in units of r_0, the (unavoidable) inner cut-off radius in the energy of a dislocation in linear elasticity theory: it was taken as b in [2–6]. The simple interpretation of the success of equation (1) in both atomic and continuum modelling is that when D is much smaller than L the screw dipole drawn out at the void when $\tau = \tau_c$ has a line tension proportional to $\ln(D)$ in elasticity theory. Conversely, when L is smaller than D the dipole of spacing L determines τ_c. The harmonic mean in the argument of the logarithm in equation (1) tends to D when D is much smaller than L and to L when L is much smaller than D.

Although atomic simulation at $T = 0$ K by molecular statics (MS) is equivalent to determining dislocation line shape in linear elasticity theory, i.e. the potential energy is minimized in both, it is striking to find that the expression for τ_c from the continuum approximation is valid for obstacles as small as a few nm in diameter.

(c) The earlier MD simulations show that τ_c decreases with increasing T. Although the line segments at the void still approach the dipole configuration at the critical stress, breakaway occurs before a true dipole is drawn out.

(d) The dislocation climbs by absorbing some vacancies from the void at breakaway at all temperatures. This effect was not predicted by earlier continuum treatments and would have to be incorporated in dislocation dynamics modelling based on elasticity theory. Monnet [16] has shown recently that the atomic-level data from [2] can be analysed in the continuum approximation to allow calculation of the dislocation–void interaction energy and determination of the dominant features in the unpinning process.

One reason for the success of equation (1) in fitting to the τ_c data from MS and MD is that the self-interaction between different parts of the dislocation line was included in [14, 15]; this effect is of course intrinsic to the atomic modelling. Also, the high Peierls stress of the screw dislocation in a BCC metal assists in stabilizing the dipole. However, the actual structure of the screw core depends on the interatomic potential used to calculate forces and energy in MS/MD simulations, and recent developments in potentials for iron make it necessary to test the validity of the work in [2–6] in that context.

It was generally accepted until recently that the core of the $1/2\langle 111\rangle$ screw dislocation in BCC iron has a degenerate structure (see references to early and later works in [17, 18]). This core has three-fold symmetry with atomic disregistry spread asymmetrically on three {110} planes of the $\langle 111\rangle$ zone. It is the core found with many pairwise and EAM-type interatomic potentials for BCC metals, including the potential for iron derived in 1997 by Ackland *et al* [19] that was used in the previous void and loop simulations [2–10]. Recent DFT calculations, however, have shown that the core has a non-degenerate structure in which disregistry is spread symmetrically on the {110} planes [20]. The more recent potential developed by Ackland *et al* [21] has this feature [22, 23]. Furthermore, it was fitted to some data that were not available in 1997 and gives better correspondence to some point defect properties, e.g. [24].

For conciseness, we shall refer to the 1997 and 2004 potentials [19, 21] as A97 and A04, respectively. It should be noted that in addition to its recent use in simulating point defects and screw dislocations in pure iron, the A04 potential is now being used for the solvent in newly developed hybrid potentials for binary ferritic alloys with metallic (Fe–Cr, Fe–Cu, Fe–Ni) and non-metallic (Fe–C, Fe–He, Fe–P) solute

elements. Thus, it is important to check whether the critical stress values, line shape and climb processes for dislocation–obstacle interactions in the A97 and A04 models are consistent with each other. In this way, it will be possible to judge whether effects found in simulation of the alloys are sensitive to the potential used for the host matrix. In this paper, therefore, we employ the A04 potential to study interaction of the $1/2\langle 111\rangle\{1\bar{1}0\}$ edge dislocation and voids of different size and spacing at different temperatures, with the aim providing direct comparison with existing and previously unpublished data obtained using the A97 potential.

3. Technique

The simulation model developed by Osetsky and Bacon [2] was employed. The principal axes x, y and z of the simulated body-centred cubic crystal were oriented along the [111], $[\bar{1}\bar{1}2]$ and $[1\bar{1}0]$ directions, respectively. The initially straight edge dislocation with slip plane x–y was created along the y direction and had Burgers vector $\boldsymbol{b} = 1/2[111]$ parallel to the x-axis (see figure 3 in [2]). Periodic boundary conditions were applied along the x and y directions. The box was divided into three parts along z. The upper and lower parts consisted of several atomic planes in which atoms were rigidly fixed in their original position, whereas atoms in the inner region were free to move in the MD cycles. A glide force on the dislocation was generated by the relative displacement of the rigid blocks in the x direction corresponding to simple shear strain ε_{xz}. The corresponding resolved shear stress induced by the applied deformation was calculated as $\tau = F_x/A_{xy}$, where F_x is the total force in the x direction on the lower outer block from all atoms in the inner region and A_{xy} is the x–y cross-section area of the box. A void (of spherical shape) with diameter D was placed in the crystal containing a relaxed edge dislocation. Its equator coincided with the dislocation slip plane. Values of D equal to 0.7, 1.0, 1.2, 1.6, 2.0 and 3.0 nm were considered. They contain 37, 59, 89, 169, 339 and 1243 vacancies, respectively.

Two model sizes were used for the simulations. The size of the inner region of the largest MD box was 119×3, 59×6 and 49×2 atomic planes along x, y and z, respectively, as in earlier works [2, 6]. The corresponding dimensions of the smaller model were 119×3, 30×6 and 25×2. The volume of these crystals was $30 \times 41 \times 20$ nm^3 and $30 \times 21 \times 10$ nm^3, and they contained just over 2 M and 0.5 M mobile atoms, respectively. The periodic distance, $(=L + D)$ was 41.2 and 21.0 nm, respectively.

For most of the simulations, strain, ε, was applied at a constant rate $\dot{\varepsilon} = 10^7$ s^{-1} to models equilibrated at temperature, T, in the range from 1 to 600 K: $T = 1$ K in these MD simulations was chosen to provide comparison with the MS simulations ($T = 0$ K) reported earlier. The steady-state velocity, v, of a dislocation on its own at this strain rate is estimated from the Orowan relation $\dot{\varepsilon} = \rho_D b v$ between strain rate and dislocation density, ρ_D, to be 23.5 m s^{-1} and 12 m s^{-1} for the large and small crystals, respectively. A few additional simulations were carried out by MD for other strain rates and by MS for $T = 0$ K for purposes of comparison, as discussed later.

Newton's equation of motion was integrated using a velocity Verlet scheme with constant time step equal to 5 and 2 fs, used for $T < 300$ K and $T \geqslant 300$ K, respectively. All calculations were done in the framework of a microcanonical NVE ensemble, where particle number, system volume and total energy are conserved if the work of external forces is taken into account. No additional temperature control was applied, for the temperature increase over the simulation time was negligible: the maximum was approximately 2 K, observed in modelling at 1 K for an accumulated strain of 3%. The physical time and number of MD time steps to complete a reaction between dislocation and void depended on T, D and MD box size. The fastest reaction occurred over 0.35 ns of MD time at 600 K for smallest void and smaller model: the longest reaction lasted more than 2 ns.

The results are described in several sections. The interaction leading to breakaway of the edge dislocation with a periodic row of voids under static (MS, $T = 0$ K) or pseudo-static (MD, $T = 1$ K) conditions is presented in section 4. The equivalent results for τ_c, line shape and breakaway mechanism under dynamic conditions (MD, $T \geqslant 100$ K) are described in section 5. Some results on crystal and dislocation properties relevant to the comparison of the A97 and A04 potentials are presented in the appendix to the paper. Finally, the results are discussed and conclusions drawn in sections 6 and 7, respectively.

4. Dislocation–void interaction at $T \leqslant 1$ K

As described in the earlier studies of this interaction with the A97 potential [2–6], the straight edge dislocation starts to glide in the model crystal at the Peierls stress, τ_P and is attracted by the void, resulting in a fall in the potential energy and applied stress τ when it cuts the entry side of the void surface. The applied stress has to be increased to τ_c to allow the dislocation to bow between the row of periodic voids so that it cuts them and breaks away. The details of this are in the references cited above and analysis of it in the continuum approximation has been presented in [16]. As shown in the appendix, although the atomic structure of the edge dislocation cores appears to be almost identical with the two potentials, there is a significant difference between the two values of τ_P. This stress is just less than 25 MPa for A97 and about 80 MPa for A04. Nevertheless, τ_c is greater than τ_P in all the cases considered and so we consider only the stress and dislocation line shape for the critical configuration.

Figure 1 shows visualizations of atoms in the dislocation core at τ_c for voids with $D = 1$, 1.6 and 2 nm in the A04 model with $L + D = 21$ nm. These critical line shapes in the glide plane are periodic in the $[11\bar{2}]$ direction and were obtained by pseudo-static MD modelling at $T = 1$ K. τ_c is 372, 490 and 530 MPa for the three D values, respectively. It is seen that much of the dislocation is aligned along the $[11\bar{1}]$ direction, implying that the Peierls stress is high for a straight dislocation of this mixed character. In fact, resistance to glide of the $[11\bar{1}]$ segment dominates bowing of the dislocation as τ is increased.

The effect of this is revealed in the τ–ε plots for $D = 1.0$, 1.2, 1.6 and 2.0 nm in figure 2. When τ exceeds τ_P the

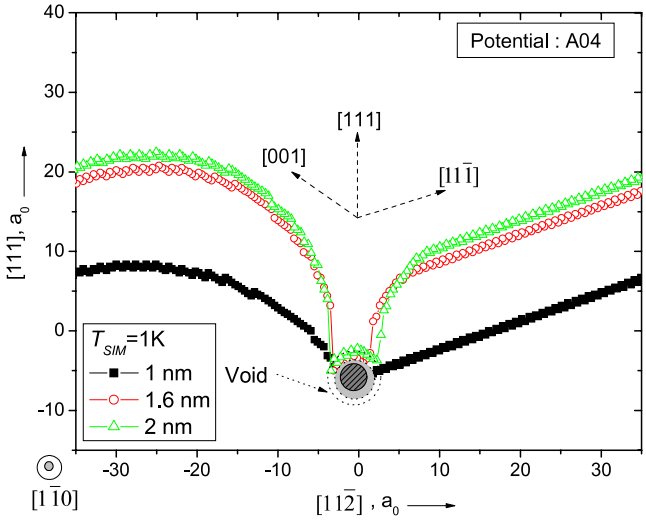

Figure 1. Dislocation line shape in the glide plane at τ_c for voids with $D = 1$, 1.6 and 2 nm in the A04 model with $(L + D) = 21$ nm.

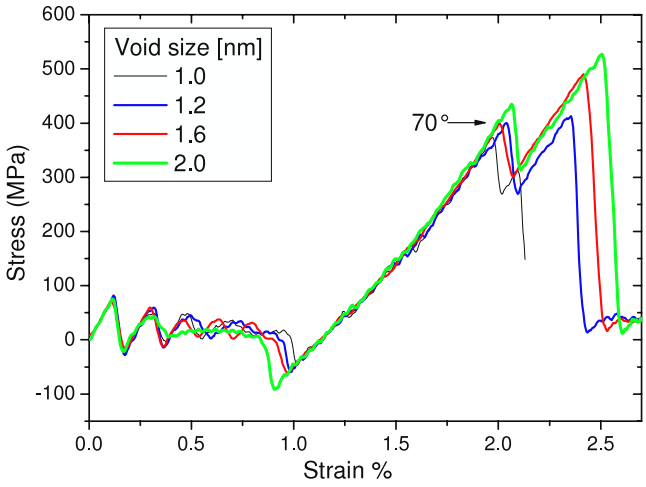

Figure 2. Stress–strain plots for four void sizes in the A04 model with $(L + D) = 21$ nm at $T = 1$ K.

initially straight dislocation starts to move forward in a series of steps under increasing strain until it is attracted into the void at $\varepsilon = 1\%$. As the applied strain increases further, a straight 70° [11$\bar{1}$] segment is formed on the bowing line and this elongates to dominate the line shape as τ approaches a maximum. All four plots exhibit two peaks in the stress before the dislocation breaks away from the periodic row of voids. The first peak at a strain of about 2% occurs as a result of the 70° segment unpinning from a void and forming a screw dipole. Note that, irrespective of D and L, the resolved shear stress required to move the [11$\bar{1}$] segment away from the void is approximately 400 MPa. Dipole formation is assisted by the mutual attraction of the two dislocation branches emerging from the void surface [14, 15]. The second peak at higher strain corresponds to final breakaway of the dipole. This becomes the critical process that determines τ_c as D increases above 1 nm, as can be seen in the critical shapes of the dislocation in figure 1.

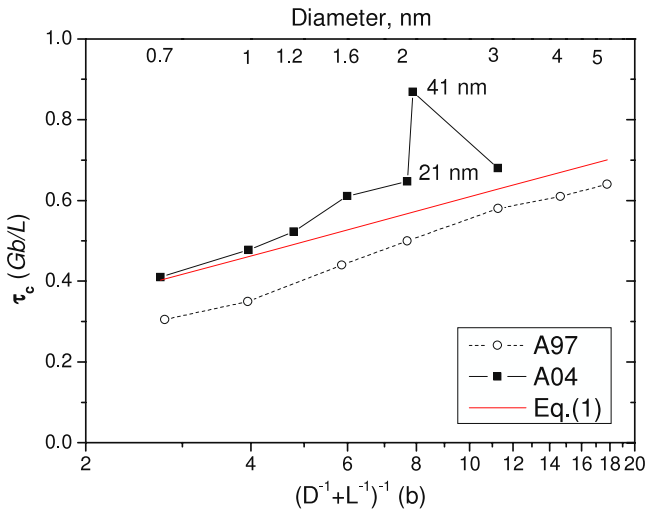

Figure 3. τ_c in units of Gb/L versus $1/(D^{-1} + L^{-1})$ on a log scale for voids of different diameter in models of the A97 and A04 potentials at 0 K and 1 K, respectively. Values given by equation (1) are also shown. The A97 simulations were obtained with $(L + D) = 41$ nm. The A04 data are for the small crystal $(L + D = 21$ nm), except for the point labelled 41 nm, which is for the larger model.

As noted in section 2, drawing out a screw dipole was also found to give rise to the critical configuration in the earlier from simulations of static conditions ($T = 0$ K) with the A97 potential. We also remark that the dislocation climbs by absorbing a few vacancies from the void at breakaway in the new simulations with the A04 potential, as in the earlier work.

The value of τ_c is plotted against $\ln[1/(D^{-1} + L^{-1})]$ in figure 3 to test the validity of equation (1). To be consistent with equation (1), τ_c is in units of Gb/L with $G = 63$ GPa, which is close to the value of the effective shear modulus for a dislocation of the 1/2[111](1$\bar{1}$0) system in iron with both potentials (see equation (A.2) of the appendix). Figure 3 also includes data for the A97 potential, some of it not published previously. (The A97 values were obtained by MS simulation ($T = 0$ K) using the larger atomic model with $(L + D) = 41$ nm.) The critical stress values for the A04 potential are consistently about 20% higher than those obtained with the A97 potential. The dependence of τ_c on L and D is similar, however, and demonstrates good agreement between τ_c obtained by atomic-level modelling and equation (1), even for small voids.

Figure 3 also contains the value of τ_c at $T = 1$ K for the 2 nm void in the A04 model with size $(L + D) = 41$ nm. It is seen to lie well away from the other data, so that τ_c obtained for a 3 nm void in the model with the smaller size is below that for a 2 nm void. The reason for this can be seen in figure 4, where the critical line shape for this case is compared with that for the same void size but smaller spacing of 21 nm. Once the [11$\bar{1}$] segment is formed in this case, it controls glide and bowing of the dislocation right up to the point when breakaway occurs. As in the case of the 1 nm void in figures 1 and 2, and unlike the critical configuration for $L = 21$ nm in figure 4, a screw dipole is not formed by attractive self-force between the

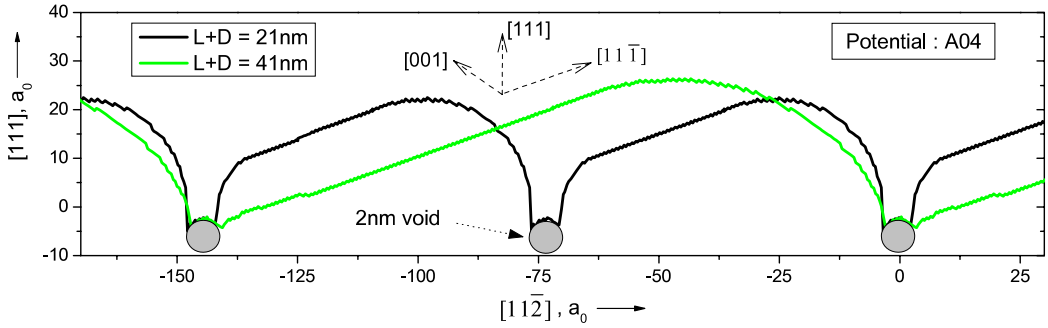

Figure 4. Dislocation line shape in the glide plane at τ_c for voids with $D = 2$ nm and $(L + D) = 21$ or 41 nm in the A04 model at $T = 1$ K.

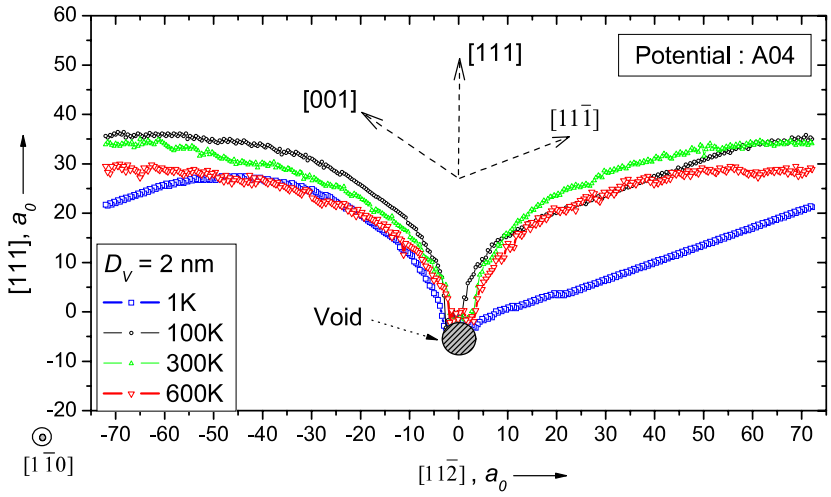

Figure 5. Dislocation line shape in the glide plane at τ_c for voids with $D = 2$ nm and $(L + D) = 41$ nm in the A04 model at $T = 1$, 100, 300 and 600 K.

dislocation branches at the void and τ_c is higher than the value for this D and L given by equation (1).

5. Dislocation–void interaction at $T \geqslant 50$ K

Dislocation line shapes in the glide plane at the critical stress for a row of voids with $D = 2$ nm and $(L + D) = 41$ nm in the A04 model at four temperatures in the range 1–600 K are shown in figure 5. It is seen that the influence of the [1 1 $\bar{1}$] line orientation, which is dominant at 1 K, is not significant at 100, 300 and 600 K. The dislocation branches that meet the void surface adopt a near-screw configuration at the three higher temperatures. A similar configuration was found at the critical stress for all the D, L and T combinations considered, although breakaway occurs before the branches reach exact parallel alignment for small values of D, i.e. before achieving true screw character. These results are consistent with those found here and in previous simulations with the A97 potential [2–6], as demonstrated in figures 6(a) and (b), where lines shapes in the critical condition for $D = 1$ nm, $(L+D) = 21$ nm are compared for the two models at $T = 100$ and 300 K. The shapes are seen to match each other closely. Furthermore, as in the modelling of $T \leqslant 1$ K, the dislocation climbs by absorbing some vacancies on leaving the void in both potential models.

The consequence of this similarity between the results of the simulations is that τ_c for a specific D, L and T combination is close to that found with the A97 and A04 interatomic potentials. This is demonstrated by the plot of τ_c versus T in figure 7. The differences are slight, except for $T \leqslant 1$ K. In addition, the effect of applied strain rate on τ_c in this temperature range is small for both interatomic potentials. This is illustrated in figure 8 for $T = 300$ K by the data for τ_c versus strain rate for voids of size $D = 1$ nm in the A04 model with $(L + D) = 21$ nm and the A97 model with $(L + D) = 41$ nm.

6. Discussion

Experiments using positron annihilation spectroscopy and small-angle neutron scattering, e.g. [25, 26], show that nano-scale cavities are formed during neutron irradiation of α-iron. Their size spectrum spans the range of void size simulated here. As noted in section 1, recent modelling [13] indicates that these cavities are possibly the most important obstacles to dislocation glide in neutron-irradiated ferritic steel. It is therefore desirable to investigate the atomic effects that occur in dislocation–void interaction and determine the obstacle strength as a function of temperature and obstacle size and spacing. Furthermore, the development of an improved interatomic potential has made it necessary for

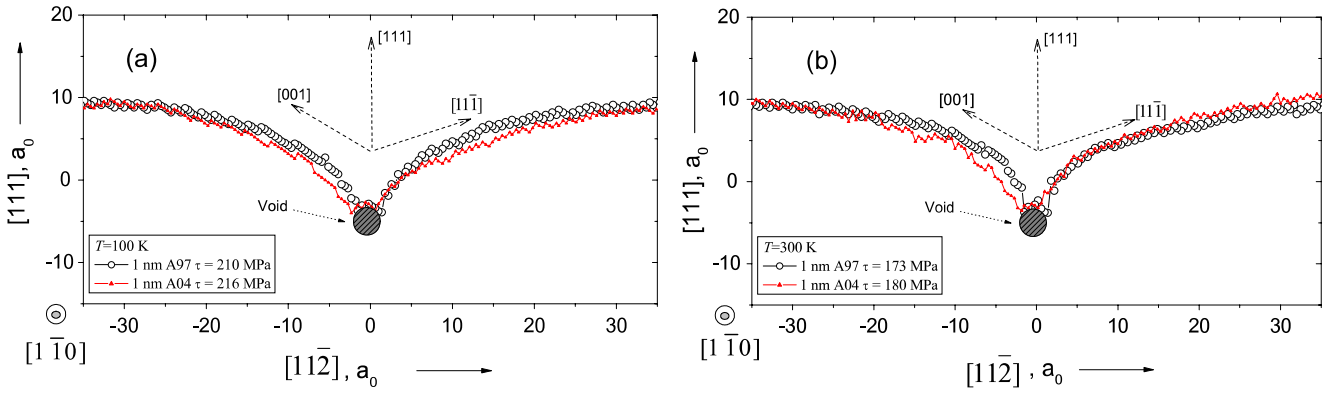

Figure 6. Comparison of the critical line shape at τ_c for $D = 1$ nm and $(L + D) = 21$ nm found with the two potentials for (a) $T = 100$ K and (b) $T = 300$ K.

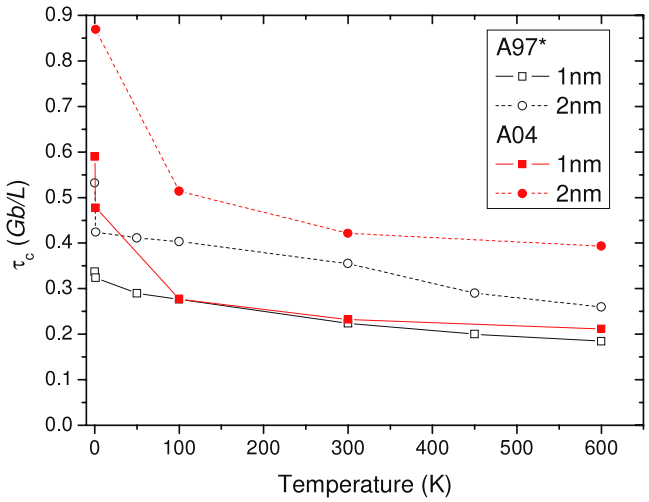

Figure 7. τ_c in units of Gb/L versus T for voids of either 1 or 2 nm diameter, as indicated. The void centre-to-centre spacing $(L + D)$ is 41 nm in all cases except for $D = 1$ nm in the A04 model.

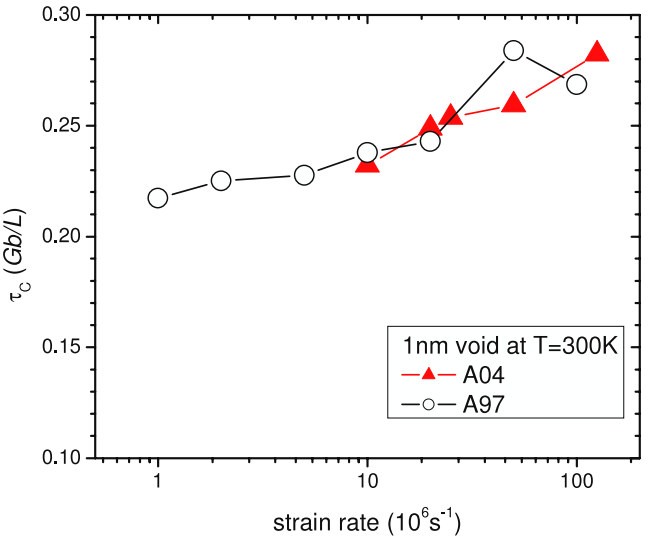

Figure 8. Variation of τ_c (units Gb/L) with applied strain rate at $T = 300$ K for $D = 1$ nm. The data for the A97 and A04 potentials are for model size $(L + D) = 41$ and 21 nm, respectively.

information gained from earlier simulations with the A97 potential [19] to be tested against results based on the newer A04 model [21]. An important conclusion of the present work is that differences in the edge dislocation–void interaction with the two potentials are not significant at temperature $\geqslant$100 K. Similar general consistency between modelling using the A97 and A04 potentials was found for edge dislocation reactions with either $1/2\langle 111\rangle$ or $\langle 100\rangle$ interstitial dislocation loops at $T \geqslant 100$ K [11, 27].

This agreement confirms the validity of the results obtained with the A97 potential in the previous MD simulations, and implies that this potential can still be used with some confidence, with the advantage of its shorter range and, therefore, computational efficiency compared with the A04 potential. It is shown in the appendix that values of the *effective* shear modulus and Poisson ratio for a dislocation of the $1/2[111](1\bar{1}0)$ system are almost the same in the two atomic models. They are close to the values obtained using anisotropic elasticity theory. This means that equations deduced in the continuum approximation, e.g. equation (1), and found to be valid with one potential should be applicable with the other.

The only significant difference found between dislocation–void interaction in the two models occurs in static (MS, $T = 0$ K) or pseudo-static (MD, $T = 1$ K) simulation. It arises from the influence of the dislocation in the 70°-mixed $[11\bar{1}]$ orientation. Although the Peierls stress, τ_P, of the pure edge dislocation is much higher for the A04 potential (see appendix) and the core configuration and glide plane of the straight screw dislocation with the A97 potential are reported to be inconsistent with *ab initio* calculation and experiment [20, 22, 23], these effects do not seem to dominate the dislocation–void interaction.

The self-stress attraction between the branches of the bowing line on opposite sides of a void assists their adoption of the screw orientation and reduces τ_c. It was shown in section 4 that this does not happen with the A04 potential at $T \leqslant 1$ K when $(L + D)$:D equals 21:1 and 41:2. In these cases, L/D is sufficiently large for τ_c, which is proportional to $1/L$, to be controlled by the Peierls stress of the 70°

dislocation. For smaller L/D, τ_c for dipole breakaway is larger than the $[11\bar{1}]$ Peierls stress and equation (1) holds. To confirm that the breakup of the $[11\bar{1}]$ segment is indeed a controlling process for the A04 model, we have performed additional static simulations for a 2 nm void. In these, the loading was started using the A97 model and continued until the dislocation reached the critical configuration (just below the critical stress necessary to shear the void). Relaxation was then continued using the A04 potential. It was observed that the straight $[11\bar{1}]$ segment was not restored and the dipole breakaway occurred at approximately the same stress as in the original relaxation performed with A04. It can therefore be concluded that the critical stress is determined by the attraction of screw arms, independently of the shape of the dislocation line connecting them.

It is not known why the Peierls stress of the 70° dislocation in $[11\bar{1}]$ orientation is so high in the A04 crystal. An atomic-level study of this dislocation in a BCC crystal was reported by Yamaguchi and Vitek [28, 29], who investigated the core structure and Peierls stress of dislocations with $\boldsymbol{b} = 1/2[111]$ in six different orientations in the $(1\bar{1}0)$ plane. Three simple pair-wise interatomic potentials were used in MS models with approximately one to two thousand moveable atoms and fixed boundary conditions parallel to the line direction. It was found that the significant inelastic displacements parallel to the Burgers vector were predominantly confined to a single $(1\bar{1}0)$ plane, except for the [111] screw. Thus, even though $[11\bar{1}]$ is a common zone axis for six different {110} and {112} planes, the core for the 70° dislocation was planar. Interestingly, however, by applying a homogeneous shear strain until the dislocation moved by a few b, the Peierls stress among the non-screw dislocations was largest for the $[11\bar{1}]$ dislocation, i.e. ∼50% larger than that of the edge dislocation for all three potentials. (The Peierls stress for the screw dislocation was 5 to 20 times that of the edge.) If the 50% factor were to apply for the A04 model, the Peierls stress would be ∼130–140 MPa. However, the evidence of figure 2 is that it is nearer to 400 MPa. Since the A97 and A04 potentials predict different core structures for the screw dislocation and significantly different values for the Peierls stress of the edge dislocation, this suggests that the core structure and corresponding Peierls stress of the $[11\bar{1}]$ mixed dislocation would also differ in the two models. The difference clearly vanishes at a temperature sufficiently high for the core structure effects to be of minor importance.

The A97 and A04 interatomic potentials used here were fitted to the same basic properties of α-iron, i.e. lattice parameter and second-order elastic constants, and similar vacancy formation energy and melting temperature. However, the two models exhibit a significant difference in properties of self-interstitial atoms, for A04 provides higher stability of the ⟨110⟩ dumbbell over the ⟨111⟩ crowdion, in agreement with *ab initio* calculations [24]. This arises mainly from differences in short-range interactions, which in turn are believed to be responsible for differences in some other static properties. For example, the edge dislocation core structure at the bottom of the extra half-plane is influenced by the structure of the SIA. Small differences in the core have been shown in the appendix to result in large differences in the static Peierls stress. They also appear to affect some dynamic properties of the edge dislocation for, as shown in figure A.4 of the appendix, the difference in the steady-state velocity of this dislocation under constant stress is large at low temperature. It is seen that the difference is reduced as T increases, and almost disappears by ∼450 K when thermal vibrations of atoms smear out the effects of fine differences in short-range interactions.

Although it is demonstrated in the appendix that τ required to maintain glide of a single edge dislocation under conditions of constant $\dot{\varepsilon}$ is higher in the A04 model than in an A97 one of the same size, it seems unlikely that this would affect the constant-$\dot{\varepsilon}$ simulations of dislocation glide and interaction with voids presented in section 5. This conclusion is reached because the maximum stress, τ_c, at which breakaway occurs is much higher than τ for steady-state glide in an obstacle-free crystal at the low $\dot{\varepsilon}$ used; i.e. steady-state velocity v from the Orowan expression $\dot{\varepsilon} = \rho_D b v$ with $\dot{\varepsilon} = 10^7\ \mathrm{s}^{-1}$ is found to be 12 and 23 m s^{-1} for the small and large MD models. The applied shear stress corresponding to this velocity is much less than τ_c.

Elastic properties are important for overall line shape in this regime. The elastic line tension, LT, is influential in determining the equilibrium line shape of dislocation segments where interaction stress from either the dislocation itself or other defects is small. It acts to reduce the curvature of a dislocation, i.e. dislocations tend to be flatter in orientations where the line tension is highest. We have therefore investigated the variation of LT with orientation of the $1/2[111](1\bar{1}0)$ dislocation using anisotropic elasticity data. When the difference in energy between edges and screws is taken into account, the line tension is [30]

$$LT = E(\theta) + \frac{\mathrm{d}^2 E(\theta)}{\mathrm{d}\theta^2}, \tag{2}$$

where $E(\theta)$ is the energy per unit length of line and θ is the angle between the line direction and a reference datum, usually taken as the direction of $\boldsymbol{b}$. The line tension for the $1/2[111](1\bar{1}0)$ system in α-iron as a function of θ measured from the [111] direction is plotted in figure 9. The data were calculated using the coefficients obtained using anisotropic elasticity theory in table 3 of [31], where the C_{ij} elastic constants for iron in [30] were used. LT is highest for the screw orientation ($\theta = 0$), as it is in most metals. It is seen that it is not the lowest for the edge orientation ($\theta = 90°$) in this case, and is actually slightly lower for the $[11\bar{1}]$ orientation. Thus, it can be concluded that alignment of the dislocation with this orientation in the low-temperature simulations with the A04 potential is not due to abnormally high elastic line tension.

It was remarked in section 3 that MD simulations for the low-temperature condition $T = 1$ K were used to mimic static conditions ($T = 0$ K) with the A04 potential and thus provide direct comparison with the MS results obtained earlier with the A97 potential. MS provides the atomistic analogue of elasticity theory in that configurations which minimize the potential energy of the system are determined. It is generally assumed that dynamic effects are minimal at 1 K. However, the influence of the high Peierls stress of the $[11\bar{1}]$ dislocation

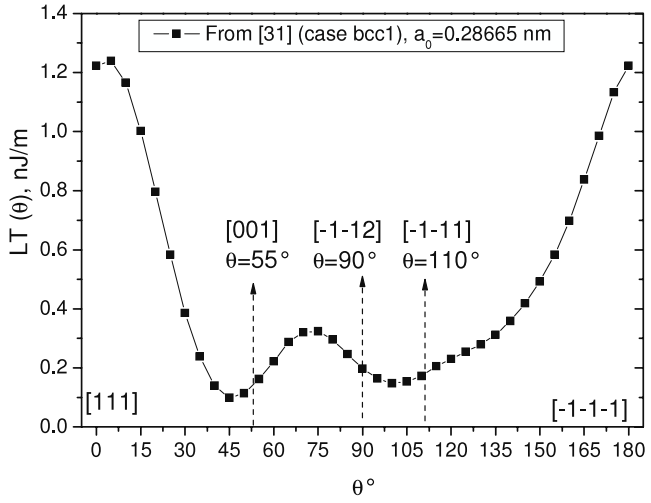

Figure 9. Variation of anisotropic elastic line tension with line orientation for a straight dislocation with $\boldsymbol{b} = 1/2[111]$ in the $(1\bar{1}0)$ plane of α-iron.

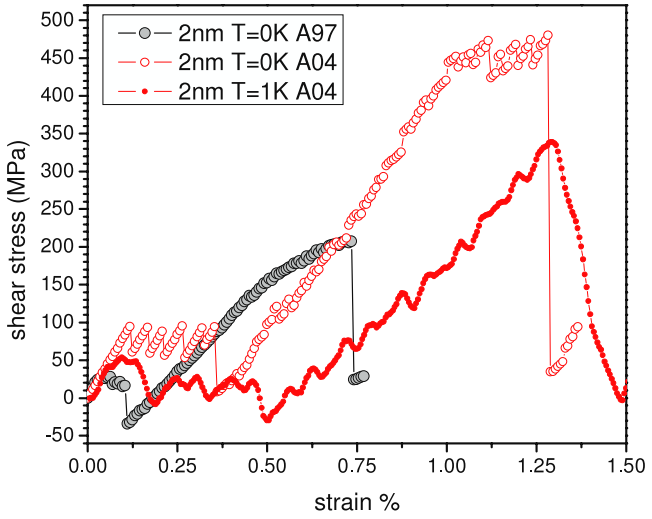

Figure 10. Comparison of shear stress versus applied shear strain for $D = 2$ nm, $(L + D) = 41$ nm in models based on the A97 (MS: $T = 0$ K) and A04 (MS: $T = 0$ K; MD: $T = 1$ K, $\dot{\varepsilon} = 10^7$ s^{-1}) interatomic potentials.

for some combinations of L and D, resulting in distinctly different results from those of the A97 model where such effects are absent, leads us to question the general assumption. Figure 10 shows τ–ε plots for the same geometry $D = 2$ nm, $(L + D) = 41$ nm. The A04 data are for $T = 1$ K (pseudo-static with $\dot{\varepsilon} = 10^7$ s^{-1}) and $T = 0$ K (true static). (The latter represents almost six CPU months on a 2.4 GHz processor.) There is significant difference between the two plots, although in both cases the process is controlled by motion of a long $[11\bar{1}]$ segment of dislocation, which breaks away from the void at τ_c. At $T = 1$ K this is the stage at which the dislocation breaks away completely (see figures 4 and 5), whereas when $T = 0$ K a short screw dipole is drawn out at constant τ before final breakaway.

The difference in τ_c between 0 and 1 K indicates that pseudo-static modelling by low-temperature MD may not be appropriate when atomic-level effects that are potential-specific dominate. Even though the applied shear strain rate was relatively low (10^7 s^{-1}) for such large-scale MD modelling, it is clear that true static conditions were not simulated in the pseudo-static case ($T = 1$ K) with the A04 potential. This can be explained as an effect of repeated motion of the dislocation over a high Peierls barrier. In this process, elastic strain energy is released at each jump forward and the relaxation due to temperature transfer by lattice vibrations into the crystal is slow at 1 K. The effective 'local' T is therefore higher than 1 K at this strain rate. This interpretation is supported by the observation that kinks were seen to be created on the screw dipole at 1 K, but not in the static simulations.

Finally, the plots in figure 10 for the A04 and A97 models at $T = 0$ K are very different. This difference, and the abrupt departure from the expected dependence of the τ_c value on D and L (figure 3) and T (figure 5) suggest the possibility that this newer potential may not be suitable for simulating static or low-temperature dislocation phenomena in iron.

7. Conclusions

Nano-scale voids are important obstacles to dislocation glide in irradiated iron. The interaction between a gliding edge dislocation of the $1/2[111](1\bar{1}0)$ slip system and spherical voids with diameter, D, in the range 0.7–3 nm and spacing, L, equal to either 21 or 41 nm has been studied by atomic-level computer simulation for temperature, T, in the range 0–600 K. The aim has been to see if conclusions obtained from previous simulations using the interatomic potential in [19] are supported by results based on the newer potential in [21]. (These potentials are identified here as A97 and A04, respectively.) The following conclusions are drawn.

(a) The core structure of the pure edge dislocation is almost the same in both models, but the Peierls stress, τ_P, at 0 K is much higher for the A04 potential. Also, the steady-state glide velocity of the edge dislocation under constant resolved shear stress is lower with this potential, particularly so for $T \leqslant 300$ K, which is consistent with the high value of Peierls stress obtained. It is also noted that simulations by others have shown that the core structure and glide plane of the $1/2\langle 111\rangle$ screw dislocation are different in the A97 and A04 models [22, 23].

(b) The present work demonstrates that differences in the edge dislocation–void interaction with the two potentials are not significant at $T \geqslant 100$ K. This is despite the fact that for large voids and/or low temperature, an initially straight edge dislocation is pulled into screw orientation by voids before dislocation breakaway. Also, the dislocation climbs by absorbing vacancies from a void during the interaction in both models. Similar general consistency between modelling using the A97 and A04 potentials has been found for edge dislocation reactions with either $1/2\langle 111\rangle$ or $\langle 100\rangle$ interstitial dislocation loops at $T \geqslant 100$ K [11, 27].

(c) This agreement confirms the validity of the results obtained with the A97 potential in the previous MD simulations [2–6], and implies that this potential, which has certain computational advantages, can be used with some confidence.

(d) The only significant difference between dislocation–void interaction in the two models occurs in static (MS, $T = 0$ K) or pseudo-static (MD, $T = 1$ K) simulation. It arises from the influence of the dislocation segment in the 70°-mixed $[11\bar{1}]$ orientation in the A04 model and is seen in the critical line shape at which the dislocation breaks form the void. It affects the critical stress, τ_c, for combinations of D and L such that $L/D \geqslant 10$. The effect on the line shape does not arise from anisotropy in the elastic line tension: it is due to high Peierls stress of this dislocation with the A04 potential.

(e) The self-stress attraction between the branches of the bowing line on opposite sides of a void assist their adoption of the screw orientation and reduce τ_c. The D- and L-dependences of τ_c then follow equation (1), which was first found by modelling the Orowan process in the approximation of linear elasticity [14].

(f) This does not apply for $T \leqslant 1$ K with the A04 potential when L/D is sufficiently large, for then τ_c, which is proportional to $1/L$, is controlled by the Peierls stress of the $[11\bar{1}]$ dislocation. It is questionable whether this potential is suitable for simulating static or low-T processes.

(g) It is shown that values of the effective shear modulus to be used in equation (1) for a dislocation of the $1/2[111](1\bar{1}0)$ system are almost the same in the two atomic models. They are close to the values obtained using anisotropic elasticity theory. This implies that equations deduced in the continuum approximation, e.g. equation (1), and found to be valid with one potential should be applicable with the other.

Acknowledgments

This work was carried out within the framework of the European Fusion Development Agreement (EFDA). It was also supported by grant GR/S81162/01 from the UK Engineering and Physical Sciences Research Council; grant F160-CT-2003-508840 ('PERFECT') under programme EURATOM FP-6 of the European Commission; and partly by the Division of Materials Sciences and Engineering and the Office of Fusion Energy Sciences, US Department of Energy, under contract DE-AC05-00OR22725 with UT-Battelle, LLC. DT thanks EDF for use of high performance computing facilities, and the authors acknowledge the provision of unpublished results by Mr Panos Grammatikopoulos.

Appendix. Crystal and straight dislocation properties with the A97 and A04 potentials

The two interatomic potentials A97 and A04 were fitted to the same set of elastic constants ($C_{11} = 243$ GPa, $C_{12} = 145$ GPa, $C_{44} = 116$ GPa) and the lattice parameter a_0 for a perfect crystal in equilibrium is almost the same in both cases (0.286 65 and 0.285 53 nm, respectively). As noted in section 2, the latter potential was fitted to data obtained by *ab initio* calculation after 1997, and so the values for the formation and migration energies of vacancies and self-interstitial atoms are superior. There appears to be no sound reason why these differences should have a significant affect edge dislocation–void interaction, although we speculate on this in section 6. The other reported difference between the two models of iron lies in the structure and preferred slip plane of the $1/2\langle 111\rangle$ screw dislocation [22, 23], and the influence of this is an issue for the current study.

Comparison of properties of the straight $1/2\langle 111\rangle\{1\bar{1}0\}$ edge dislocation in the two crystal models has not been given previously. Figure A.1(a) shows the variation of the difference, $\Delta(u_x)$, of the displacement component u_x between atoms in atomic planes above and below the glide plane when the potential energy is minimized. This is a well-known way of representing the spread of disregistry associated with a planar dislocation core [33]. The derivative, $\mathrm{d}(\Delta u_x)/\mathrm{d}x$, which gives the distribution of Burgers vector in the glide plane, is shown in figure A.1(b). These plots show that although the core is slightly wider in the A97 model, the difference is not such that a significant difference in dislocation behaviour under stress would be expected.

Additional information on the core and energy of a dislocation can be obtained from MS simulation by plotting the potential energy stored within cylinders of radius R centred on the dislocation core. Plots for the edge and screw dislocations are shown in figure A.2. (The screw dislocation along [111] was created in a model with size 30 nm in the $[\bar{1}\bar{1}2]$ and $[1\bar{1}0]$ directions using the boundary conditions [22], i.e. free surfaces in the $[\bar{1}\bar{1}2]$ direction.) The non-linearity for small R arises from the atomic disregistry in the dislocation core. The core radius measured in this way is approximately the same for both dislocations with both potentials, i.e. ∼2–3b. The variation of strain energy outside the core cylinder should correspond to the functional dependence given by linear elasticity:

$$E(R) - E(r_0) = Kb^2 \ln\left(\frac{R}{r_0}\right). \qquad \text{(A.1)}$$

The factor K equals $G/4\pi$ and $G/4\pi(1-\nu)$ for screw and edge dislocations, respectively, in isotropic elasticity, where G is the shear modulus and ν is Poisson's ratio. It was shown in [15, 34] that in order to match the strength of voids and impenetrable obstacles in the isotropic elasticity approximation to that obtained by a full anisotropic elasticity calculation, *effective* G and ν values can be estimated from K given by anisotropic elasticity theory for straight screw and edge dislocations. The values obtained by using equation (A.1) for the linear parts of the plots in figure A.2 are

$$A97: G = 65 \text{ GPa}, \qquad \nu = 0.499. \qquad \text{(A.2}a\text{)}$$

$$A04: G = 62 \text{ GPa}, \qquad \nu = 0.488. \qquad \text{(A.2}b\text{)}$$

The inset plot of $(1 - E_{\text{screw}}/E_{\text{edge}})$ versus R in figure A.2 shows there is a slight variation of the effective Poisson's ratio with R, but it is close to the value given in equation (A.2)

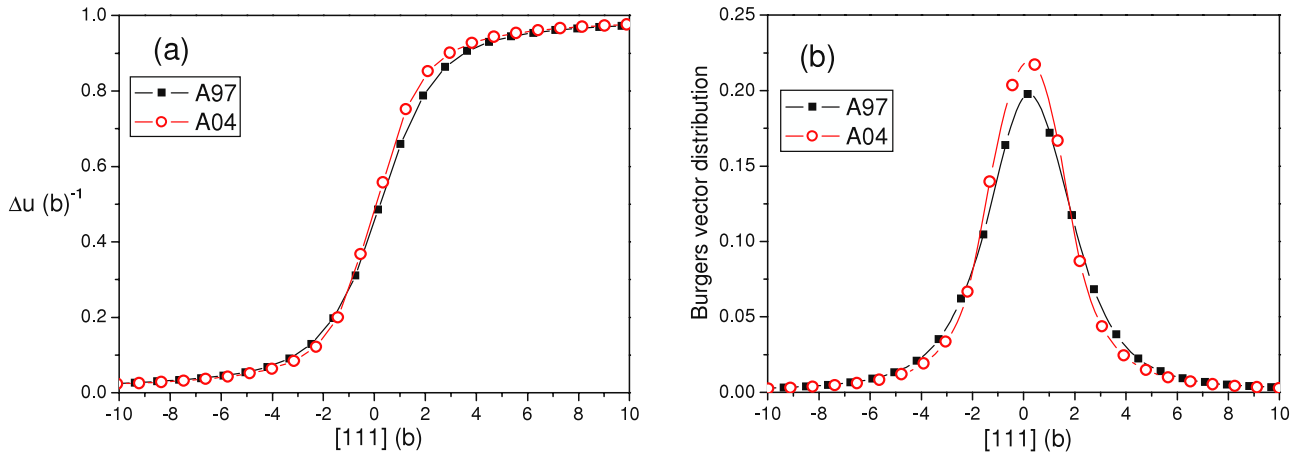

Figure A.1. (a) Difference of the displacement component u_x between atoms across the $(1\bar{1}0)$ slip plane as a function of x for an edge dislocation in the two models. (b) Derivative of Δu_x with respect to x, showing the Burgers vector distribution in the slip plane [32].

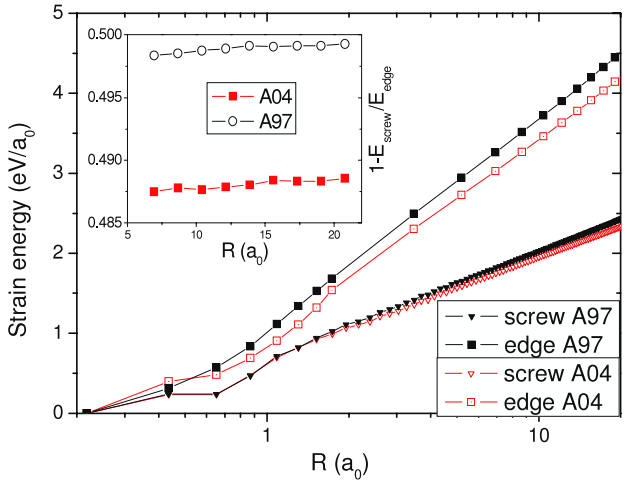

Figure A.2. Variation with R of the potential energy in a circular cylinder of radius R centred on the dislocation core for screw and edge dislocations in atomic models based on the A97 and A04 potentials. The inset plot shows the variation of the effective Poisson's ratio with R.

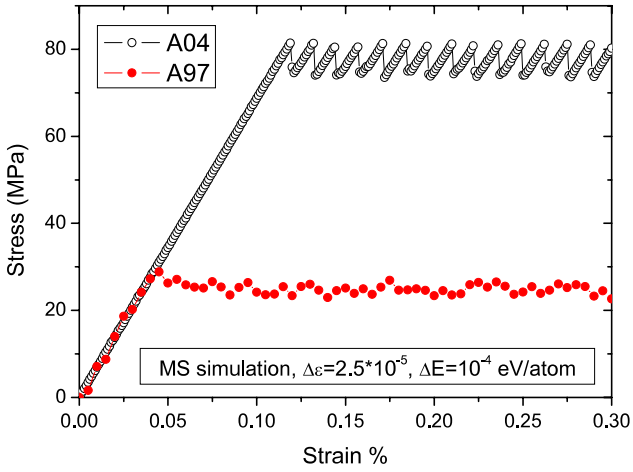

Figure A.3. Shear stress versus shear strain for a model containing a single edge dislocation at $T = 0$ K. The dislocation glides at the Peierls stress τ_P equal to about 25 and 90 MPa for the A97 and A04 crystals, respectively.

for both models. The effective constants in equation (A.2) compare with $G = 63$ GPa and $\nu = 0.47$ presented in [35] after [15, 34], where slightly different C_{ij} values were used from those to which the interatomic potentials were fitted ($C_{11} = 242$ GPa, $C_{12} = 147$ GPa, $C_{44} = 112$ GPa [30]). It is apparent, therefore, that neither the core structure nor the surrounding strain energy of the straight edge dislocation exhibits unexpected differences between the two potentials.

Despite the similarity in core structure, the Peierls stress of the straight edge dislocation, τ_P, i.e. the critical resolved shear stress at which the dislocation glides at $T = 0$ K, is much higher in the A04 model of iron. This is shown in figure A.3, where shear stress versus shear strain at $T = 0$ K is plotted for both potentials. These plots were obtained by applying strain in increments of 2.5×10^{-5} and relaxing the crystal after every increment to minimize the potential energy to an energy convergence of better than 10^{-4} eV/atom. τ_P is seen to be about 25 MPa for the A97 model and 90 MPa for the newer

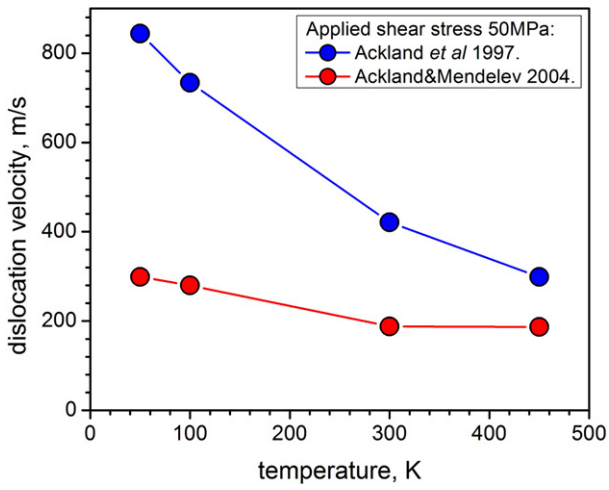

Figure A.4. Velocity of an edge dislocation as a function of temperature in a crystal under constant applied shear stress $\tau = 50$ MPa.

A04 potential. The origin of this large difference is not known: it is not apparent from inspection of the atomic disregistry in the core region or the distribution of Burgers vector described above.

In light of this result, we have also looked for differences in the glide behaviour of the two edge dislocations under dynamic conditions ($T > 0$ K). As an example, figure A.4 shows the steady-state glide velocity, v, as a function of temperature for an edge dislocation in a crystal under a constant applied resolved shear stress of 50 MPa. The velocity decreases with increasing T due to phonon damping in both models, but is much smaller with the A04 potential. The factor of three difference at low T presumably arises from the same cause as the difference in τ_P.

References

[1] Harry T and Bacon D J 2002 *Acta Mater.* **50** 195
Harry T and Bacon D J 2002 *Acta Mater.* **50** 209
[2] Osetsky Yu N and Bacon D J 2003 *Model. Simul. Mater. Sci. Eng.* **11** 247
[3] Osetsky Yu N, Bacon D J and Mohles V 2003 *Phil. Mag.* **83** 3623
[4] Osetsky Yu N and Bacon D J 2003 *J. Nucl. Mater.* **323** 268
[5] Bacon D J and Osetsky Yu N 2005 *Mater. Sci. Eng.* A **400/401** 353
[6] Osetsky Yu N and Bacon D J 2005 *Mater. Sci. Eng.* A **400/401** 374
[7] Jumel S, Van Duysen J-C, Ruste J and Domain C 2005 *J. Nucl. Mater.* **346** 79
[8] Rong Z, Osetsky Yu N and Bacon D J 2005 *Phil. Mag.* **85** 1473
[9] Bacon D J, Osetsky Yu N and Rong Z 2006 *Phil. Mag.* **86** 3291
[10] Bacon D J and Osetsky Yu N 2007 *J. Met.* **59** 42
[11] Terentyev D, Malerba L, Bacon D J and Osetsky Yu N 2007 *J. Phys.: Condens. Matter* **19** 456211
[12] Spitzig W A and Keh A S 1970 *Acta Metall.* **18** 611
[13] Queyreau S 2008 *Thèse de Doctorat de* l'Université Pierre et Marie Curie, Paris
[14] Bacon D J, Kocks U F and Scattergood R O 1973 *Phil. Mag.* **28** 1241
[15] Scattergood R O and Bacon D J 1982 *Acta Metall.* **30** 1665
[16] Monnet G 2007 *Acta Mater.* **55** 5081
[17] Duesbery M S and Vitek V 1998 *Acta Mater.* **46** 1481
[18] Vitek V 2004 *Phil. Mag.* **84** 415
[19] Ackland G J, Bacon D J, Calder A F and Harry T 1997 *Phil. Mag.* A **75** 713
[20] Frederiksen S L and Jacobsen K W 2003 *Phil. Mag.* **83** 365
[21] Ackland G J, Mendelev M I, Srolovitz D J, Han S and Barashev A V 2004 *J. Phys.: Condens. Matter* **16** S2629
[22] Domain C and Monnet G 2005 *Phys. Rev. Lett.* **95** 215506
[23] Chaussidon J, Fivel M and Rodney D 2006 *Acta Mater.* **54** 3407
[24] Willaime F, Fu C-C, Marinica M C and Dalla Torre J 2005 *Nucl. Instrum. Methods Phys. Res.* B **228** 92
[25] Eldrup M and Singh B N 2003 *J. Nucl. Mater.* **323** 346
[26] Bergner F, Ulbrich A, Gokhman A and Erak D 2008 *J. Nucl. Mater.* **373** 199
[27] Terentyev D, Grammatikopoulos P, Bacon D J and Osetsky Yu N 2008 *Acta Mater.* **56** 5034
[28] Yamaguchi M and Vitek V 1973 *J. Phys. F: Met. Phys.* **3** 523
[29] Vitek V and Yamaguchi M 1973 *J. Phys. F: Met. Phys.* **3** 537
[30] Hirth J P and Lothe J 1982 *Theory of Dislocations* (New York: Wiley)
[31] Bacon D J and Scattergood R O 1974 *J. Phys. F: Met. Phys.* **4** 2126
[32] Grammatikopoulos P 2008 University of Liverpool, unpublished work
[33] Hull D and Bacon D J 2001 *Introduction to Dislocations* 4th edn (Oxford: Butterworth-Heinemann)
[34] Scattergood R O and Bacon D J 1974 *Phil. Mag.* **31** 179
[35] Bacon D J 1985 in *Fundamentals of Deformation and Fracture* ed B A Bilby, K J Miller and J R Willis (Cambridge: Cambridge University Press) pp 401–15